Engineering Geology 193 (2015) 412–420

Contents lists available at ScienceDirect

Engineering Geology

journal homepage: www.elsevier.com/locate/enggeo

Spatial monitoring of groundwater drawdown and rebound associated with quarry dewatering using automated time-lapse electrical resistivity tomography and distribution guided clustering

J.E. Chambers [a,*], P.I. Meldrum [a], P.B. Wilkinson [a], W. Ward [b], C. Jackson [a], B. Matthews [c], P. Joel [c], O. Kuras [a], L. Bai [b], S. Uhlemann [a,d], D. Gunn [a]

[a] Geophysical Tomography Team, British Geological Survey, Nottingham NG12 5GG, UK
[b] University of Nottingham, School of Computer Science & Information Technology, Nottingham NG8 1BB, UK
[c] Lafarge Tarmac, Stancombe Lane, Flax Bourton, Bristol BS48 3QD, UK
[d] ETH-Swiss Federal Institute of Technology, Institute of Geophysics, Sonneggstr. 5, 8092 Zurich, Switzerland

ARTICLE INFO

Article history:
Received 9 March 2015
Received in revised form 9 May 2015
Accepted 12 May 2015
Available online 16 May 2015

Keywords:
Electrical resistivity tomography (ERT)
Mining
Dewatering
Groundwater monitoring
Clustering
Image analysis

ABSTRACT

Dewatering systems used for mining and quarrying operations often result in highly artificial and complex groundwater conditions, which can be difficult to characterise and monitor using borehole point sampling approaches. Here automated time-lapse electrical resistivity tomography (ALERT) is considered as a means of monitoring subsurface groundwater dynamics associated with changes in the dewatering regime in an operational sand and gravel quarry. We considered two scenarios: the first was unplanned interruption to dewatering due to a pump failure for a period of several days, which involved comparing ALERT monitoring results before and after groundwater rebound; the second involved a planned interruption to pumping over a period of 6 h, for which near-continuous ALERT monitoring of groundwater rebound and drawdown was undertaken. The results of the second test were analysed using distribution guided clustering (DGC) to provide a more quantitative and objective assessment of changes in the subsurface over time.

ALERT successfully identified groundwater level changes during both monitoring scenarios. It provided a more useful indication of the rate of water level rise and maximum water levels than piezometer monitoring results. This was due to the piezometers rapidly responding to pressure changes at depth, whilst ALERT/DGC provided information of slower changes associated with the storage and delayed drainage of water within the sediment. By applying DGC we were able to automatically and quantitatively define changes in the resistivity sections, which correlated well with the direct observations of groundwater at site. For ERT monitoring applications that generate numerous time series, the use of DGC could significantly enhance the efficiency of data interpretation, and provide a means of automating groundwater monitoring through assigning alarm thresholds associated with rapid changes in groundwater conditions.

1. Introduction

Quarry dewatering requires careful groundwater management, using extraction boreholes, ponds, trenches and well-point systems (Wardrop et al., 2001). This can result in highly artificial and dynamic groundwater conditions that can present challenges both for quarry management and the protection of groundwater resources outside of the mineral extraction operations (Brunetti et al., 2013; French, 2009; Mayes et al., 2005). Monitoring approaches typically rely on manual or automated measurements of groundwater levels in boreholes or surface waters. However, borehole monitoring networks provide sparsely distributed point information, which in complex settings can be insufficient to understand the groundwater system.

Geophysical monitoring approaches have the potential to complement conventional point monitoring by providing spatial information relating to changing groundwater conditions (e.g., Binley et al., 2002; Kuras et al., 2009). Electrical resistivity tomography (ERT) is of particular relevance due to the close relationship between resistivity and pore saturation and pore fluid quality (e.g., Binley et al., 2002; Brunet et al., 2010). This coupled with recent advances in monitoring instrumentation (e.g., Ogilvy et al., 2009; Wilkinson et al., 2010; Chambers et al., 2014a; Supper et al., 2014) and time-lapse inversion techniques (e.g., Hayley et al., 2011; Karaoulis et al., 2011; Kim et al., 2009; Loke et al., 2014) have facilitated automated remote monitoring activities relating to a range of hydrogeophysical applications (Loke et al., 2013). However, to the best of our knowledge these automated approaches

* Corresponding author.
E-mail address: jecha@bgs.ac.uk (J.E. Chambers).

http://dx.doi.org/10.1016/j.enggeo.2015.05.015
0013-7952/

have not yet been developed for application to quarry dewatering activities. An additional challenge for the application of automated ERT monitoring is the very large or numerous time series data sets generated by these systems, which are difficult to process manually. Automated image analysis using computer vision techniques such as gradient based edge detectors (e.g., Chambers et al., 2012, 2013; Elwaseif and Slater, 2012; Hsu et al., 2010) and clustering techniques (e.g., Audebert et al., 2014; Chambers et al., 2014b; Ward et al., 2014) is beginning to be applied to ERT images. For time-series data these techniques have the potential to provide an automated means of interrogating monitoring results.

In this study, we aim to assess a combination of automated time-lapse electrical resistivity tomography (ALERT) and distribution guided clustering (DGC) as a means of monitoring groundwater dynamics in an active quarry with well-point dewatering. Two monitoring scenarios are considered; the first concerns an extended unplanned interruption to quarry dewatering monitored using ALERT, and the second is a planned interruption to pumping, which was monitored at a higher temporal resolution using a combination of ALERT and DGC to provide detailed information on groundwater rebound and subsequent drawdown over a much shorter time period. Resistivity monitoring results are compared to direct observations of groundwater levels within the monitoring boreholes, and the potential benefits of image analysis for the automated interpretation of resistivity images are considered.

2. Site description

Rock Common Quarry (Fig. 1) is located approximately 11 km to the north of Worthing, West Sussex (British National Grid reference 512500, 113500). Quarrying activity has been concentrated in the Folkestone Formation of the Lower Greensand Group (Cretaceous), which dips to the south beneath the clays of the Gault Formation (Cretaceous). The Folkestone Formation comprises fine to medium, and occasionally coarse, cross-bedded sand. This formation is underlain by the Sandgate and Hythe Beds, also of the Lower Greensand Group, which in the area of Rock Common Quarry include a fine grained upper unit called the Marehill Clay.

The quarry has been worked since the 1920s, and at the time of this study extended to a depth of approximately 40 m at its deepest point. In recent years dewatering of the quarry has been carried out using well-point arrays (e.g., Shaqour and Hasan, 2008; Chiocchini and Castaldi, 2011) connected to a network of pumps installed across the base of the quarry. This has been supplemented with extraction from ponds or sumps at times of higher rainfall. The well-point system comprises linked arrays of shallow boreholes from which groundwater is abstracted using a network of pumps. For this quarry the well-point extraction boreholes extended to 5 m below ground level and were positioned at approximately 2 m intervals (Figs. 1 and 2). Continuous pumping maintained the water level between approximately 0.5 to 2 m below the lowest point of the quarry floor during normal conditions, and approximately 20 m below the naturally occurring water table observed in the land surrounding the quarry. The hydrological regime was extremely dynamic, with flash flooding across the quarry floor due to heavy rainfall events particularly during winter months. Likewise, groundwater levels have been observed to be very sensitive to changes in the pumping regime; e.g., when pumping is reduced groundwater rebounds of tens of centimetres occur within a few hours.

The monitoring array was installed within the deepest part of the quarry (Fig. 1). This location was chosen for a number of reasons: (1) it was in close proximity to the pump control cabin that was used to house the ALERT system; (2) it was within an area of the quarry that was not going to be significantly impacted or disturbed by quarrying operations for the duration of the study; (3) it was directly adjacent to one of the active well-point groundwater extraction array, thereby providing the opportunity to observe groundwater drawdown and rebound directly associated with small changes to the pumping regime. Routine monitoring at the site was undertaken at the site over a period of 12 months, during which ERT measurement sets were typically collected at a frequency of one per day, though periods of higher frequency monitoring were also undertaken to monitor the active interruption to pumping.

3. Methodology

3.1. Monitoring scenarios

Two contrasting monitoring scenarios were considered in this study, the first of which involved changes between equilibrium conditions at high and low water levels monitored at a low temporal resolution, and the second concerned dynamic, continually changing conditions monitored at higher temporal resolution.

Scenario 1 involved an unplanned interruption to groundwater extraction resulting from the failure of one of the quarry pumps for a period of 5 days during April 2010. Water extraction continued at a

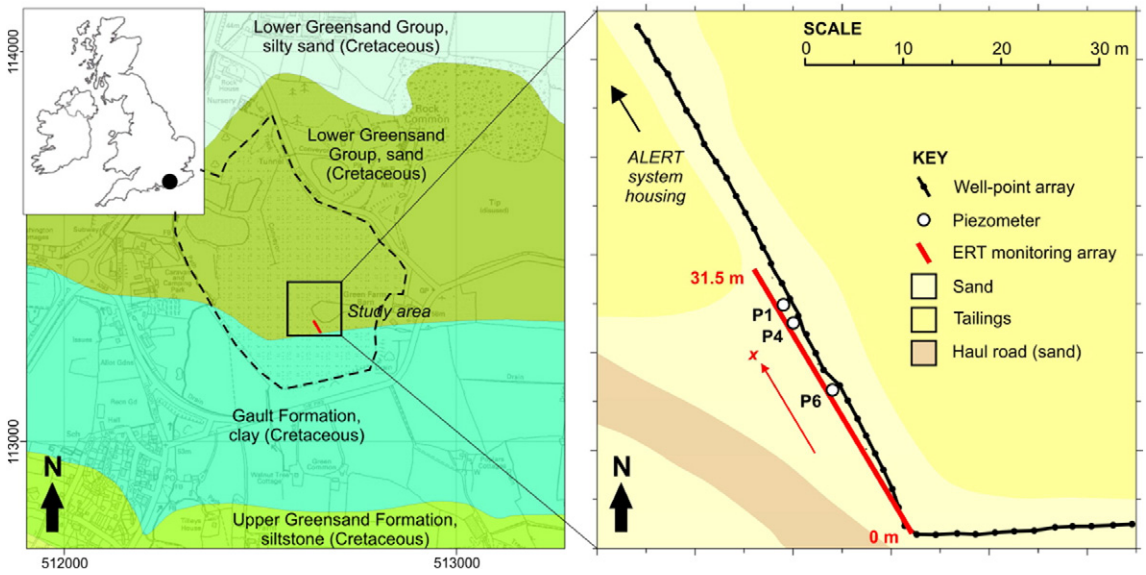

Fig. 1. Setting — geological map with Ordnance Survey base layer (© Crown copyright and database rights 2015 Ordnance Survey 100021290), showing quarry boundary (dashed black line) and the study site location, with site location at national scale inset (left). Schematic field layout showing monitoring array, piezometers and well-point system (right).

Fig. 2. ALERT instrument installation (left). Electrode monitoring array installation (right) — the well-point groundwater extraction system can be seen running parallel to the electrode array.

reduced rate for this period, during which groundwater levels rapidly reached a new equilibrium state at a higher elevation within the subsurface. ALERT results are compared before and after pump failure.

Scenario 2 concerned a planned temporary pump switch off for a period of ~6 h during May 2010. The purpose of this test was to monitor the rebound and subsequent drawdown of groundwater levels using the ALERT system operating at a much greater temporal resolution, with near-continuous monitoring being undertaken immediately before, during and after pump switch-off.

3.2. Automated time-lapse electrical resistivity tomography (ALERT)

3.2.1. Instrumentation

The resistivity distribution in the subsurface was monitored using an ALERT system (Fig. 2), which is described in detail by Ogilvy et al. (2009) and Wilkinson et al. (2010). In brief, the system uses wireless telemetry (a wireless cellular router in this case) to communicate with a database management and control system located on a remote server (Fig. 3). This system controls the scheduling, storage, inversion and delivery of the data and resulting tomographic images. Once installed, no manual intervention is required; data is transmitted automatically according to a pre-programmed schedule and specific survey parameters, both of which can be modified remotely as conditions change. The system is powered by 12 V batteries, which were charged at this site using mains power. It is a 200 W direct current (DC) resistivity system and supports 10-channel simultaneous potential difference measurements

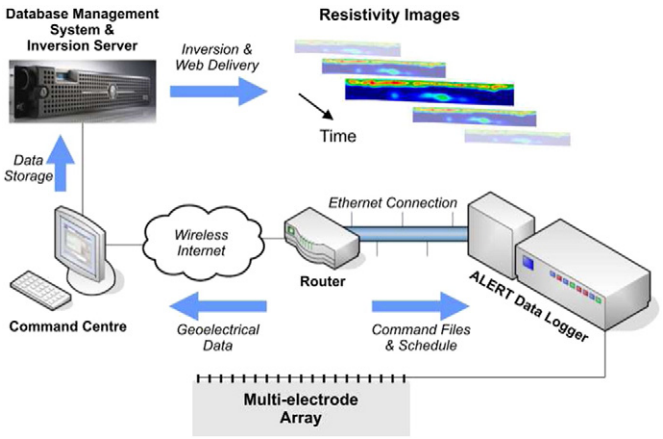

Fig. 3. ALERT system concept showing both site (multi-electrode array, data logger, router) and office based components (command centre and server). Wireless telemetry is used to schedule measurements at the remote field site, which are automatically undertaken and transferred back to the command centre. Data retrieved from the field site are stored on the server and processed to generate resistivity image time-series.

The resistivity monitoring array comprised 64 electrodes positioned at 0.5 m intervals. The array was constructed using stainless steel rod electrodes, which were connected to the ALERT instrument by multi-stranded cable arrays. The array was positioned within a shallow trench, no more than 15 cm deep, which was backfilled after installation (Fig. 2). Electrodes were bedded with a small quantity of clay (kaolin), which was intended to reduce contact resistances and maintain a good galvanic contact between the ground and the electrodes.

3.2.2. Data collection, processing and inversion

A 64-electrode dipole–dipole array (normal and reciprocal) with dipole sizes (a) of 0.5, 1, 1.5, 2, 2.5, 3, 3.5, and 4 m, and dipole separations (na) with n = 1 to 8 was used for monitoring the unplanned interruption to pumping (Scenario 1).

For the planned interruption (Scenario 2) a subset of the array was used comprising 48-electrodes (x = 8 to 31.5 m) and a dipole–dipole array (normal and reciprocal) with dipole sizes (a) of 0.5, 1, 1.5, 2, and 2.5 m, and dipole separations (na), n = 1 to 10 was used. By reducing the number of electrodes and dipole sizes measurement time was reduced (i.e., from 160 min to 50 min per set) thereby improving the temporal resolution and reducing motion blur (Rucker, 2014) during a period of rapidly changing groundwater levels associated with the pumping experiment.

Time-lapse inversion of the ERT time-series data was undertaken using an L_1-norm time constraint (Kim et al., 2009; Karaoulis et al., 2011). A robust constraint (L_1-norm) was imposed on the resistivity model, and on the data discrepancy to minimise the effects of outlying data. Prior to inversion data with a reciprocal error of >5% were removed (Wilkinson et al., 2012). The agreement between the modelled and observed data was generally very good, with mean absolute differences converging to < 1.3% for Scenario 1 and <0.9% for Scenario 2.

3.3. Automated image analysis

For this study DGC was applied to define resistivity changes associated with water level rise. It has previously been successfully applied to resistivity image analysis (e.g., Chambers et al., 2014b), and is adapted here for use with time-lapse data to highlight subtle change over time. In this case clustering is applied to the log resistivity ratio ($\log(\rho_i/\rho_0)$) rather than the log resistivity ($\log(\rho)$). The method for DGC is extended from that described in Ward et al. (2014) for clustering volumes of differing resistivity in temporally stationary ERT models. This approach is based on the probability density of the data on a log scale.

To define regions, and assign data, some measure of similarity must first be declared. Typically, for so-called centroid-based clustering

methods, data is assigned to a cluster based on some distance measured between each datum and the geometric mid-point (i.e., centroid) of the cluster. Each datum is assigned to a cluster based on minimising the distance to its centroid so that each group is made up of the close neighbourhoods in the dataset.

It is common to first define the number of clusters based on some user observation and input, then centroids for each cluster are generated in some manner, e.g., random assignment. For the *k*-means method, some *k* defined centroids are used to initialise the data into groups. From these groups, new geometric centres are found by means of a weighted average. The new set of centroids is used to re-sort the data and this process of updating and reassignment is repeated until some convergence criteria are met.

To avoid this approach of random initialisation, and remove the necessity of an iterative scheme for solving the clustering problem, it is possible to incorporate known information about the data. One such approach is to approximate the probability distribution function of the data. This can be used to identify distinct modal regions representing regions with similar values within the data. Modelling these regions by fitting normal distributions gives statistical information about likely clusters, which can be used directly in the assignment (Fig. 4). The number of modelled distributions also corresponds to the number of clusters.

For each cluster, a function can be defined to assign some measure of "membership" of each datum in the model:

$$u_i(r) = \left[\sum_{j=1}^{k}\left(\frac{d_i(r)}{d_j(r)}\right)^2\right]^{-1} \quad (1)$$

$$d_i(r) = |r-\bar{r}_i|(1-G_i(r)).$$

Subscripts *i* and *j* correspond to the index of a cluster and its distribution information $1 \le i, j \le k$. G_i refers to the fitted normal for that *i*th cluster/modal region centred on mode $\bar{r}_i$. σ^2 is the variance calculated for the mode.

$$G_i(r) = \exp\left(-\frac{(r-\bar{r}_i)^2}{2\sigma_i^2}\right) \quad (2)$$

To cluster the time-lapse model, which is made up of a collection of ERT models (in this case 2D slices), the clustering was applied to the collection as a whole. The assignment was applied to each point, independent of spatial and temporal information, and resulting cluster indices mapped back to their corresponding positions and times.

3.4. Direct groundwater monitoring

An array of piezometers was installed to provide calibration and validation for the ALERT monitoring data. Three piezometers were used during this study, which are referred to as P1, P4, and P6, extending to 1.61 m, 1.42 m, and 1.86 m below ground level (bgl) respectively (Fig. 1). The holes were fully screened, with the lower 1 m comprising slotted well screen. Each piezometer was instrumented with a groundwater level logger (Solinst Level Logger Gold M5), which was set to record a measurement at 5 minute intervals. The sampling interval was reduced to 60 s during the planned interruption to pumping.

4. Results

4.1. Scenario 1: unplanned interruption

The failure of the pump during the unplanned interruption resulted in a significant rise in groundwater levels. The levels recorded in piezometers P1 and P6 (Fig. 5) rose from 0.9 m and 1.5 m bgl to 0.3 m and 0.2 m above ground level respectively during the period of reduced pumping. Although water levels in the piezometers rose above ground level the quarry floor was not flooded during the event. This is because these levels are indicative of the change in the pressure head over the screened section of the piezometers, and not of the movement of the phreatic surface. This response has also been observed in a number of nearby open well-points.

The changing moisture content associated with the rise in groundwater level was clearly seen in the ALERT data. The monitoring 'snapshot' in Fig. 6, shows the changes in resistivity between the initial (t_a) and reduced (t_b) pumping regime. Although changes are clearly seen in the resistivity sections, their extent and magnitude are most clearly defined in the log resistivity ratio plot, which removes the geological heterogeneity that is included in the resistivity sections. The dark blue linear feature in the ratio plot, representing a decrease in resistivity, shows the area of the section that went from unsaturated to saturated. The bottom of this feature therefore defines the pre-interruption water level, whereas the top defines the raised water level. The lower level in particular shows significant variability that may be related to differences in the performance of the respective well-points (i.e., due to silting up or local variation in the permeability of the formation). The lower level defined in the resistivity images corresponds closely to the level indicated by the water level loggers in P1 and P6, i.e., ~0.9 and 1.2 m bgl respectively. There is, however, a slight discrepancy between the upper groundwater level defined by the logger and the ERT section. The water level indicated by ALERT in this case closely matches the true water level, which was visually observed at or just below the ground surface.

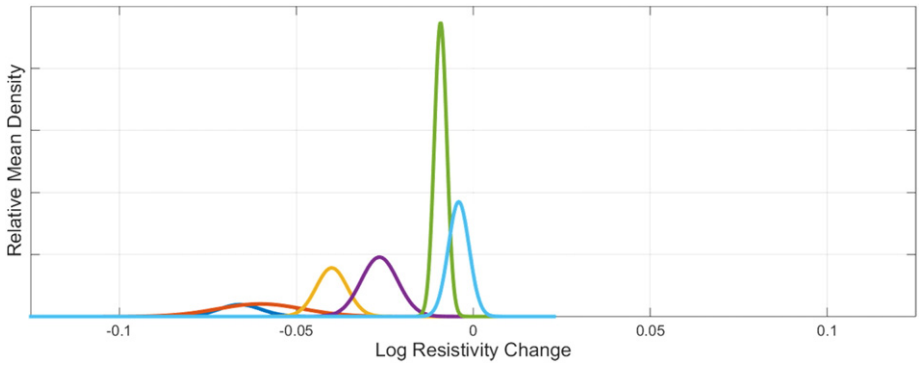

Fig. 4. Normal distributions fitted to the mean density function of Rock Common quarry log resistivity ratio model, created by summing the density function at each time slice and dividing by the total number. Each independent distribution forms the distance and centroid information for a cluster.

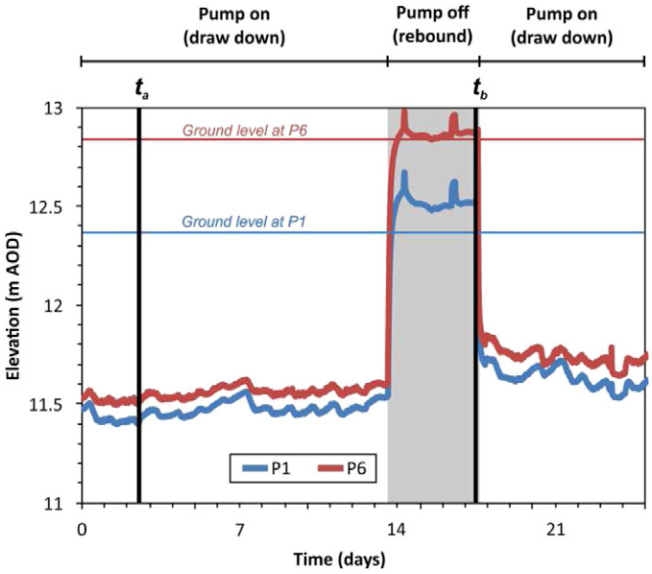

Fig. 5. Groundwater level records for piezometers 1 and 6 for the period of the unplanned interruption to pumping (Scenario 1). Shaded region indicates period of pump failure.

The feature defining the rise in water level is concentrated between $x = 6$ and 28 m. At each end of the section this feature is either poorly defined or absent. There are a number of potential reasons for this observation. The first is that diminishing image resolution towards the end of the lines has prevented water table change being detected in these areas. Secondly, it may be due to limited resistivity change towards the ends of the section related to either an elevated water table or compositional differences associated with the presence of clay minerals. Small scale variations in water level are indicated throughout the imaging sections (e.g., at $x = 17$ m), and could be related to the variable performance of individual well points or due to proximity to the southern limit of the well point array (i.e., $x = 0$ m) where groundwater head gradients are likely to be greater — however, this does not explain the lack of change towards $x = 31.5$ m. Compositional differences towards the end of the section are probably more relevant. A greater concentration of clay minerals (e.g., due to mixing or local peaks in the elevation of the top surface of the Marehill Clay) would reduce the magnitude of resistivity changes due to greater water retention in the fine grained material and electrical conduction on the clay mineral surfaces. The resistivity sections indicate that the Marehill Clay is very close to the surface in this area of the quarry floor, as evidenced by low resistivity material (i.e., clay) underlying a thin (~0–2 m) higher resistivity surface layer (sand) observed in fully saturated conditions (Fig. 6, t_b), and is particular close to the surface towards the ends of the sections.

4.2. Scenario 2: planned interruption to pumping

During the planned pump switch-off ground water levels rebounded by up to ~0.9 m as recorded by the groundwater level loggers (Fig. 7). Water level change was also indicated by ALERT monitoring, shown in Fig. 8 as time-lapse resistivity and log resistivity ratio sections, and in Fig. 9 as plots of the log resistivity ratio principal cluster distributions.

The mean density function calculated for the ratio image was modelled with distributions for 6 distinct populations, as shown in Fig. 4. Note that major regions in the relative density were located about 0 log ratio change, which correspond to the regions of little

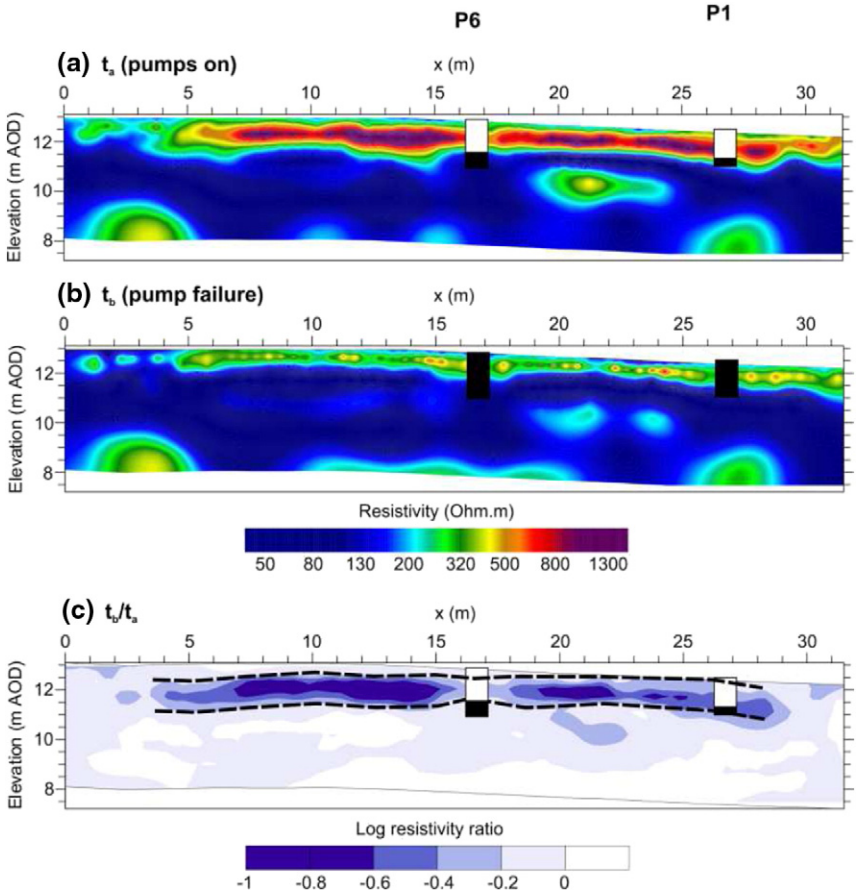

Fig. 6. ALERT monitoring results for the unplanned interruption to pumping (Scenario 1) at (a) t_a and (b) t_b (see Fig. 5), and (c) log resistivity ratio plot (t_b/t_a) showing subsurface change. Water levels shown for peizometers P1 and P6. Dashed lines show the minimum and maximum water levels estimated from the log resistivity ratio section.

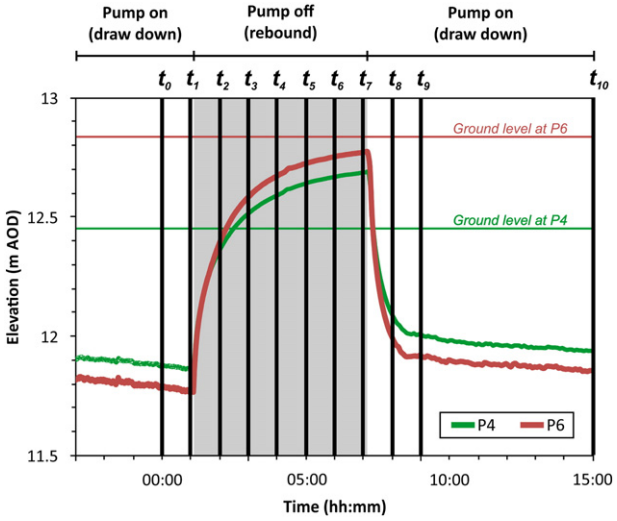

Fig. 7. Groundwater level records for piezometers 4 and 6 for the period of the planned interruption to pumping (Scenario 2). Shaded region indicates period during which pumping was reduced.

change within the image. The regions with largest negative changes represent the areas where there was a large drop in resistivity from the baseline — the corresponding cluster is then most likely to identify the area through which the water table rises.

Using the fitted distributions for the distance function described in (2), data within the entire ratio image can be given membership values for each cluster. Each datum is assigned the cluster index for which u_i is maximised. From the resulting clustering, by taking the boundary of some major cluster that is non-background and represents the greatest magnitude change, a contour can be created that highlights significant resistivity change from the baseline. The results of this contouring, taken around the cluster representing the maximum absolute change is shown Fig. 9. The threshold range captured by the major cluster is log resistivity ratio [−0.546, −0.064]. The volume of the principal cluster at each time slice is plotted in Fig. 10 along with the piezometer monitoring records of P4 and P6, showing the increase in the volume of the saturated zone that gradually decreases back to baseline level after the pump was switched back on.

Although ground moisture changes observed with ERT are in broad agreement with the piezometer data, level changes indicated by the resistivity monitoring appear to lag those recorded in the piezometers — e.g., see Figs. 8 and 9, t_2 (rise lag) and t_8 (fall lag). The lag between ERT derived change and piezometer results is also shown in Fig. 10, where the major cluster area change shows a significant lag particularly during the drawdown phase. Moreover, the artesian levels observed in the boreholes were not observed across the ground surface — confirming that water level rise in the piezometers proceeded more rapidly than the saturation of the surrounding material. Minor water seepages at the ground surface were observed in the vicinity of P1 and P4 from t_4, providing direct confirmation of water level, which agreed very well with ERT and DGC derived groundwater levels. The greatest rebound in groundwater level is seen towards $x = 8$ m, which marks the southern limit of the well-point system and is the closest part of the array to the quarry edge and, hence, the steepest hydraulic gradients.

4.3. Discussion

4.3.1. Comparison of scenarios 1 and 2

Comparison of the log resistivity ratio sections shows that the magnitude of the resistivity changes associated with groundwater level change was greater for Scenario 1 (Fig. 6) than for Scenario 2 (Fig. 8). Establishment of equilibrium conditions over a period of several days during pump failure may have provided more time for the sediment in Scenario 1 to become saturated as air entrained in the pore space was lost. In addition, near equilibrium conditions established in Scenario 1 eliminated motion blur effects (e.g., Rucker, 2014), whereas in Scenario 2 significant level changes occurred during the time it took to collect a measurement set, which would inevitably result in temporal and spatial blurring of the image. A consequence of this would be smoothing and potential underestimation of the peak resistivity changes during water level rise.

Temperature changes are not thought to have significantly affected the resistivity results in either scenario. Temperature records from the water level data loggers recorded changes of less than 1 °C for each test period, which would have a negligible impact on resistivity (Hayley et al., 2007). Moreover, given the brevity of the tests (i.e., 16 days for Scenario 1 and 4 days for Scenario 2) seasonal temperature variations will have had little influence. Similarly, diurnal temperature changes will have only effected the top few centimetres of the subsurface (e.g., Chambers et al., 2014a) with little influence on ALERT results.

4.3.2. Direct versus non-invasive monitoring

Three principal differences can be observed between the direct (water level logger) and non-invasive (ALERT) monitoring approaches: (1) spatial and temporal resolution; (2) water level response times to changes in pumping; (3) maximum water level elevation.

The temporal resolution (or sampling frequency) that can be achieved using water level loggers is very much greater than can be achieved for resistivity monitoring (i.e., seconds verses tens of minutes). Likewise, the vertical resolution of the in-hole loggers is considerably greater (i.e., sub-centimetric verses decimetric). The ALERT results provide only an approximate indication of the rise and fall of water levels. In particular, water level rise at t_2 in Scenario 2 is observed towards $x = 8$ m (Fig. 8), with little indication of rise towards $x = 32$ m despite borehole water levels having increased at both ends. It is likely that the rise towards $x = 32$ m was too small to be resolved. However, at the following time step (t_3) the water level rise has extended across the right hand side of the section towards $x = 32$ m as the newly saturated layer became thick enough to be resolved. A key advantage of ERT monitoring is that greater horizontal resolution can be achieved, with the results in this case indicating significant variability in degree of saturation and magnitude of rebound across the section. Further benefits are likely to be realised for larger scale deployments with sparser borehole distributions.

The piezometers responded more rapidly to changes in the pumping regime than the ALERT monitoring results (Fig. 8). This was observed during the rebound phase (pumping off), but was particularly marked during the drawdown phase (pumping on) (Fig. 10). The piezometers react quickly to the onset and cessation of extraction because they respond predominantly to the change in the *pressure head* in the system, which propagates rapidly through the saturated aquifer; the speed of this response is controlled by the hydraulic conductivity of the sediments, and by the compressibility of the matrix and of water, termed *specific storage*. By contrast, the changes in the resistivity images are caused by the changes in the degree of saturation of the pore space of the unsaturated zone above the phreatic surface. This is a slower process because the storage associated with wetting up or drainage of pores, the *specific yield*, is typically a number of orders of magnitude greater than that of specific storage. In this case the ALERT and DGC results have provided a more representative record of true subsurface moisture changes compared to piezometer records. The piezometers respond very rapidly to changes in pressure head, but over the periods of the extraction borehole pumping/recovery tests, they are not indicative of wetting up/drying of the unsaturated zone and the associated movement of the water table.

The maximum water levels observed in the boreholes exceeded the maximum levels observed by ALERT monitoring in both Scenarios 1 and 2. Direct visual observations of the ground surface confirmed that maximum water levels were at or just below ground level, whereas the

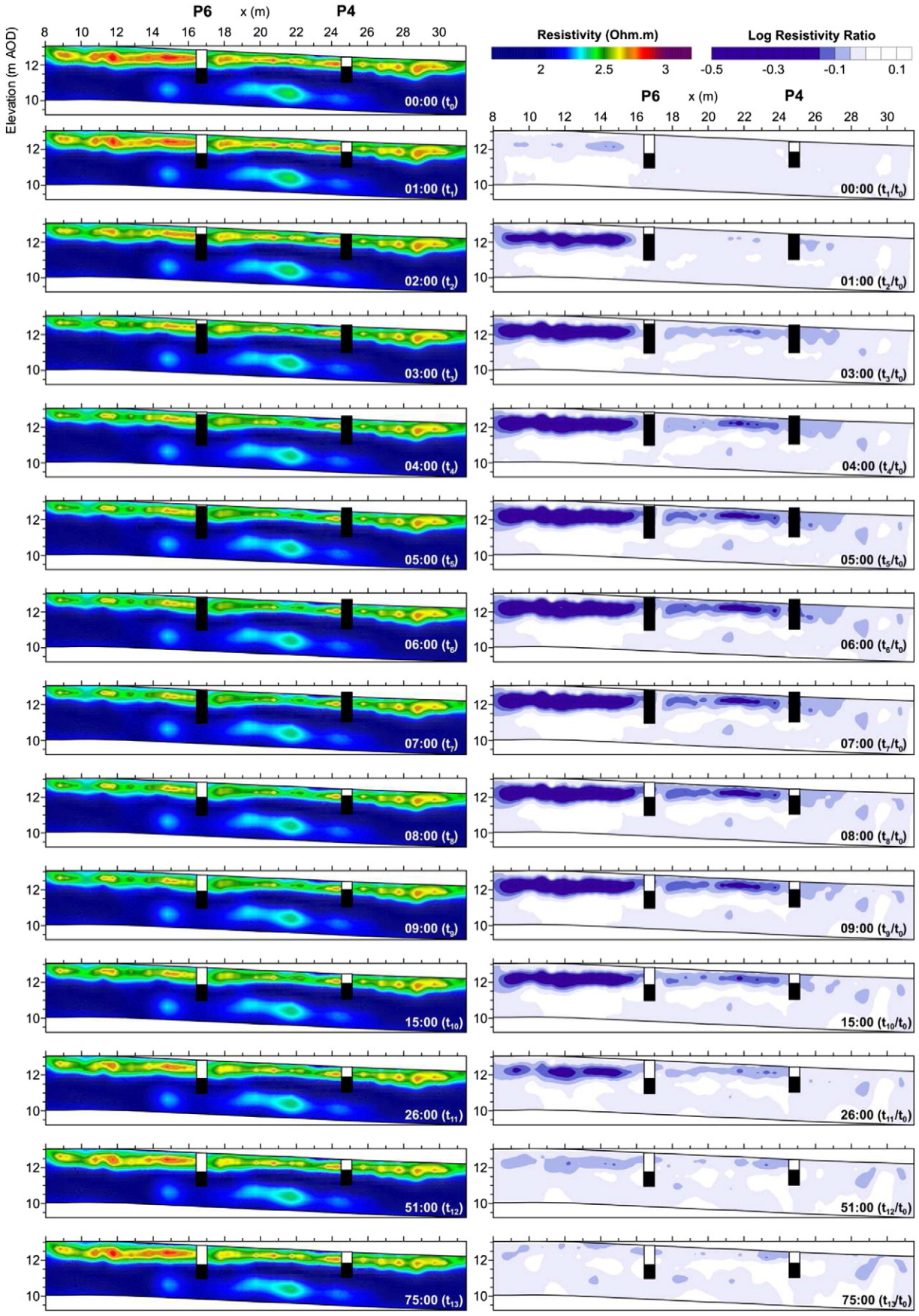

Fig. 8. Left column — resistivity monitoring results for the planned interruption to pumping (Scenario 2) between t_0 and t_{13} (see Fig. 7). Right column — log resistivity ratio plots showing change from t_1 and t_{13} relative to base line conditions, t_0. Time is given as hours and minutes (hh:mm). Water levels shown for peizometers P4 and P6.

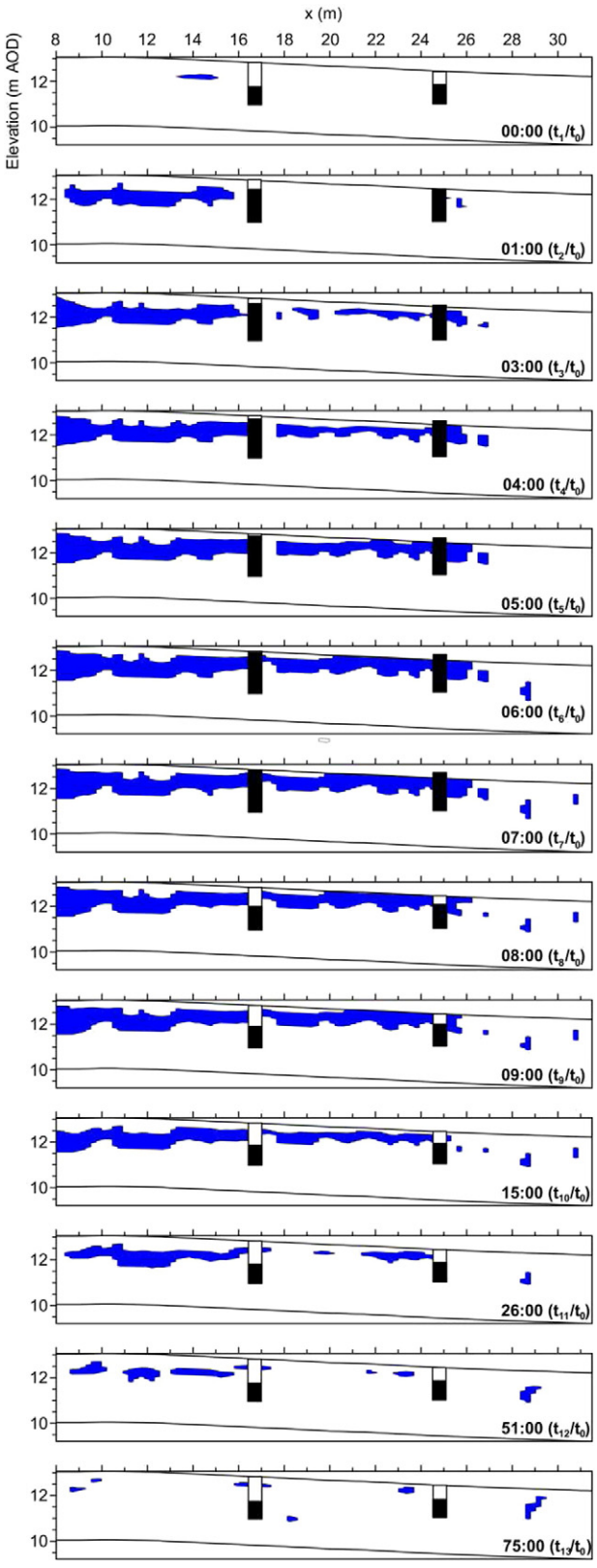

Fig. 9. Contour plots of major change cluster from t_0 to t_{13}, with water level records for piezometers 4 and 6.

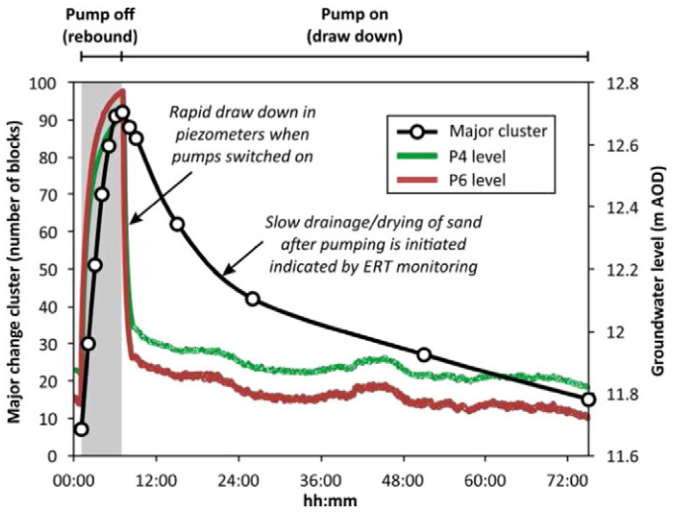

Fig. 10. Major change cluster area verses water level records from piezometers 4 and 6 during the planned interruption to pumping (Scenario 2). Shaded region indicates period during which pumping was reduced.

piezometers displayed artesian levels (Figs. 5 and 7). The ALERT/DGC results were consistent with these observations (Figs. 6, 8 and 9), and therefore provided a more useful indication of subsurface moisture conditions than the piezometers. The discrepancy between piezometer and ALERT records for Scenario 2 can be explained by the lag between the pressure response observed in the boreholes compared to the slower changes in sediment saturation detected in the resistivity images. However, for Scenario 1, where new steady state conditions were established after pump failure, the piezometric head observed in the boreholes did not equilibrate with the water levels in the sediment (this is supported from visual observations on the quarry floor and the ALERT/DGC monitoring results) — even after a period of several days (Figs. 5 and 6). This may be due to semi-confined behaviour of the shallow aquifer due to lower permeability materials near the surface. In the vicinity of the arrays cemented sands were observed at the ground surface along with clayey materials washed in from previous flood events, which would have had a lower permeability than the underlying unconsolidated sands. It should also be noted that groundwater conditions in the quarry were highly artificial, with significant topographic variability, and continued pumping in other areas of the quarry during Scenarios 1 and 2. This included groundwater extraction from a surface pond ~40 m to the northwest of the ALERT electrode array, which could have also significantly influenced subsurface flow conditions.

4.3.3. Automated interpretation of ERT monitoring

Distribution guided clustering provides a means of automatically detecting and quantifying spatial changes within ERT images. In this case DGC successfully identified the zone in which water levels rose (validated with reference to initial levels observed in the boreholes and observations of maximum water levels at the ground surface). Manual intervention was required at the outset to select the principal cluster that corresponded best to the observed level changes — however, after selection of the cluster, image analysis can be automatically applied across the whole time series. For ongoing monitoring applications it is anticipated that alarm thresholds linked to change areas automatically detected by DGC could be used to generate alarms indicating significant changes in groundwater conditions.

5. Conclusions

Groundwater monitoring using ALERT has revealed significant spatial changes in subsurface sediments related to changes in the dewatering regime in an active quarry. In particular, resistivity change images and DGC results have been useful for identifying pre-rebound water levels, which correlated well with levels in observation wells, and peak groundwater levels, which correlated well with observations at the ground surface (i.e., seepages and very shallow excavations). A

significant lag was observed between piezometer and ALERT derived groundwater responses during rebound and drawdown, which we have attributed to the slower wetting up or drying out of unsaturated zone, and associated movement of the water table, compared to the more rapid pressure head change response observed in the piezometers. Crucially, for peak water levels the ALERT monitoring results provided a more reliable means of estimating water level than the piezometers — this was probably due to semi confined aquifer conditions affecting water levels in the boreholes. DGC provided a means of quantitatively assessing changes in the log resistivity ratio sections; this approach, which requires no manual intervention once the principal change cluster has been identified, will allow the automated interrogation of resistivity monitoring data for long term monitoring operations.

Acknowledgements

The research was funded by Defra through the MIST Programme (grant MA/7/G/1/007), and in-kind contributions from project partners. The authors wish to thank the project partners for their contributions to the project. This paper is published with the permission of the Executive Director of the British Geological Survey (NERC).

References

Audebert, M., Clément, R., Touze-Foltz, N., Günther, T., Moreaua, S., Duquennoi, C., 2014. Time-lapse ERT interpretation methodology for leachate injection monitoring based on multiple inversions and a clustering strategy (MICS). J. Appl. Geophys. 111, 320–333.

Binley, A., Cassiani, G., Middleton, R., Winship, P., 2002. Vadose zone flow model parameterisation using cross-borehole radar and resistivity imaging. J. Hydrol. 267 (3-4), 147–159.

Brunet, P., Clement, R., Bouvier, C., 2010. Monitoring soil water content and deficit using Electrical Resistivity Tomography (ERT) — a case study in the Cevennes area, France. J. Hydrol. 380, 146–153.

Brunetti, E., Jones, J.P., Petitta, M., Rudolph, D.L., 2013. Assessing the impact of large-scale dewatering on fault-controlled aquifer systems: a case study in the Acque Albule basin (Tivoli, central Italy). Hydrogeol. J. 21, 401–423.

Chambers, J.E., Wilkinson, P.B., Wardrop, D., Hameed, A., Hill, I., Jeffrey, C., Loke, M.H., Meldrum, P.I., Kuras, O., Cave, M., Gunn, D.A., 2012. Bedrock detection beneath river terrace deposits using three-dimensional electrical resistivity tomography. Geomorphology 177, 17–25.

Chambers, J.E., Wilkinson, P.B., Penn, S., Meldrum, P.I., Kuras, O., Loke, M.H., Gunn, D.A., 2013. River terrace sand and gravel deposit reserve estimation using three-dimensional electrical resistivity tomography for bedrock surface detection. J. Appl. Geophys. 93, 25–32.

Chambers, J.E., Gunn, D.A., Wilkinson, P.B., Meldrum, P.I., Haslam, E., Holyoake, S., Kirkham, M., Kuras, O., Merritt, A., Wragg, J., 2014a. 4D electrical resistivity tomography monitoring of soil moisture dynamics in an operational railway embankment. Near Surf. Geophys. 12, 61–72.

Chambers, J.E., Wilkinson, P.B., Uhlemann, S., Sorensen, J.P.R., Roberts, C., Newell, A.J., Ward, W.O.C., Binley, A., Williams, P.J., Gooddy, D.C., Old, G., Bai, L., 2014b. Derivation of lowland riparian wetland deposit architecture using geophysical image analysis and interface detection. Water Resour. Res. 50, 5886–5905.

Chiocchini, U., Castaldi, F., 2011. The impact of groundwater on the excavation of tunnels in two different hydrogeological settings in central Italy. Hydrogeol. J. 19, 651–669.

Elwaseif, M.E., Slater, L., 2012. Improved resistivity imaging of targets with sharp boundaries using an iterative disconnect procedure. J. Environ. Eng. Geophys. 17, 89–101.

French, C., 2009. Hydrological monitoring of an alluviated landscape in the lower Great Ouse valley at Over, Cambridgeshire: the quarry restoration phase. Environ. Archaeol. 14, 62–75.

Hayley, K., Bentley, L.R., Gharibi, M., Nightingale, M., 2007. Low temperature dependence of electrical resistivity: Implications for near surface geophysical monitoring. Geophys. Res. Lett. 34.

Hayley, K., Pidlisecky, A., Bentley, L.R., 2011. Simultaneous time-lapse electrical resistivity inversion. J. Appl. Geophys. 75, 401–411.

Hsu, H.L., Yanites, B.J., Chen, C.C., Chen, Y.G., 2010. Bedrock detection using 2D electrical resistivity imaging along the Peikang River, central Taiwan. Geomorphology 114 (3), 406–414.

Karaoulis, M.C., Kim, J.-H., Tsourlos, P.I., 2011. 4D active time constrained resistivity inversion. J. Appl. Geophys. 73 (1), 25–34.

Kim, J.-H., Yi, M.-J., Park, S.-G., Kim, J.G., 2009. 4-D inversion of DC resistivity monitoring data acquired over a dynamically changing earth model. J. Appl. Geophys. 68, 522–532.

Kuras, O., Pritchard, J.D., Meldrum, P.I., Chambers, J.E., Wilkinson, P.B., Ogilvy, R.D., Wealthall, G.P., 2009. Monitoring hydraulic processes with automated time-lapse electrical resistivity tomography (ALERT). Compt. Rendus Geosci. 341, 868–885.

Loke, M.H., Chambers, J.E., Rucker, D.F., Kuras, O., Wilkinson, P.B., 2013. Recent developments in the direct-current geoelectrical imaging method. J. Appl. Geophys. 95, 135–156.

Loke, M.H., Dahlin, T., Rucker, D.F., 2014. Smoothness-constrained time-lapse inversion of data from 3D resistivity surveys. Near Surf. Geophys. 12, 5–24.

Mayes, W.M., Large, A.R.G., Younger, P.L., 2005. The impact of pumped water from a de-watered Magnesian limestone quarry on an adjacent wetland: Thrislington, County Durham, UK. Environ. Pollut. 138, 443–454.

Ogilvy, R.D., Meldrum, P.I., Kuras, O., Wilkinson, P.B., Chambers, J.E., Sen, M., Pulido-Bosch, A., Gisbert, J., Jorreto, S., Frances, I., Tsourlos, P., 2009. Automated monitoring of coastal aquifers with electrical resistivity tomography. Near Surf. Geophys. 7, 367–375.

Rucker, D.F., 2014. Investigating motion blur and temporal aliasing from time-lapse electrical resistivity. J. Appl. Geophys. 111, 1–13.

Shaqour, F.M., Hasan, S.E., 2008. Groundwater control for construction purposes: a case study from Kuwait. Environ. Geol. 53, 1603–1612.

Supper, R., Ottowitz, D., Jochum, B., Kim, J.-H., Roemer, A., Baron, I., Pfeiler, S., Lovisolo, M., Gruber, S., Vecchiotti, F., 2014. Geoelectrical monitoring: an innovative method to supplement landslide surveillance and early warning. Near Surf. Geophys. 12, 133–150.

Ward, W.O.C., Wilkinson, P.B., Chambers, J.E., Oxby, L.S., Bai, L., 2014. Distribution-based fuzzy clustering of electrical resistivity tomography images for interface detection. Geophys. J. Int. 197, 310–321.

Wardrop, D.R., Leake, C.C., Abra, J., 2001. Practical techniques that minimize the impact of quarries on the water environment. Trans. Inst. Min. Metall. Sect. B Appl. Earth Sci. 110, B5–B14.

Wilkinson, P.B., Meldrum, P.I., Kuras, O., Chambers, J.E., Holyoake, S.J., Ogilvy, R.D., 2010. High-resolution Electrical Resistivity Tomography monitoring of a tracer test in a confined aquifer. J. Appl. Geophys. 70, 268–276.

Wilkinson, P., Loke, M.H., Meldrum, P.I., Chambers, J.E., Kuras, O., Gunn, D.A., Ogilvy, R.D., 2012. Practical aspects of applied optimised survey design for Electrical Resistivity Tomography. Geophys. J. Int. 189, 428–440.